Transition Metal Chemistry (2024) 49:75–86
https://doi.org/10.1007/s11243-023-00563-6

Preparation, characterization and electrochemical properties of ruthenium carbonyl octaethylporphyrins with axial quinoline and quinine ligands

Dennis Awasabisah[1] · Jack F. Gangemi[1] · Douglas R. Powell[2] · Guoxing Lin[3]

Received: 15 August 2023 / Accepted: 30 October 2023 / Published online: 21 November 2023

Abstract

The six-coordinate ruthenium(II) porphyrin complexes (OEP)Ru(CO)(Q), (OEP = 2,3,7,8,12,13,17,18-octaethylporphyrinato dianion; Q = quinoline, Qnl (**2**); quinine, QN (**3**)) have been prepared from (OEP)Ru(CO) (**1**) and characterized by MS, IR, UV–visible and ^{1}H NMR spectroscopy. The X-ray crystal structure of **2** has been determined, which reveals quinoline coordination to Ru through the nitrogen atom. In the crystal packing of **2**, the two Qnl groups of adjacent porphyrins are positioned relatively parallel to each other at a close distance of 3.30 Å, implying a relatively strong π-π interaction. The X-ray crystal structure of **1** was obtained, which revealed coordination of the water to the ruthenium center. By comparing the spectroscopic data for **1**, **2** and **3**, it was determined that the site of binding of QN to Ru is likely through the nitrogen atom of the quinoline moiety. The redox behavior of the complexes at a Pt working electrode studied in a CH_2Cl_2 solution with NBu_4PF_6 as support electrolyte by cyclic voltammetry revealed oxidations that are porphyrin-centered.

Introduction

Quinoline-based compounds have important biological applications ranging from anti-cancer agents [1], anti-inflammatory [2] and antimalarial agents [3]. When used as antimalarials, quinoline-based drugs such as quinine, chloroquine and mefloquine are believed to inhibit hemozoin formation by interacting with the prosthetic heme group of hemoglobin [4], as well as the hemozoin crystals [5]. The mechanism of the hemozoin inhibition process has been the subject of interest in recent years [6]. The heme group is the most common target of many antimalarial drugs especially during the pathogenic asexual blood stage level of the life cycle of the *Plasmodium* parasite [7]. As a result, efforts have been made to fully understand the mechanism by which heme activates antimalarials.

In the literature, several spectroscopic techniques [8–12], computational methods [13, 14] and X-ray crystallography [11] have been used to shed light on the role of the antimalarial drugs in inhibiting hemozoin. In this work, we were interested in preparing relatively stable synthetic heme model-antimalarial adducts to help us characterize them spectroscopically, determine their solid-state structures, and study their electrochemical behavior. Ruthenium(II) porphyrin carbonyls are good candidates for this purpose, since generally they are low-spin, diamagnetic and relatively more stable than the iron species [15]. Due to the larger d-orbitals of Ru compared to Fe, a stronger metal-to-ligand backbonding is expected in ruthenium(II) porphyrin carbonyls, thus allowing for easy isolation and characterization of products. Although chemically different from the iron(II) counterpart, this robust nature of the ruthenium(II) complexes has allowed researchers to use Ru in place of Fe to model the properties of (por)Fe active sites [16–18].

Traditionally, ruthenium(II) porphyrin complexes (e.g. ruthenium porphyrin nitrosyls) [19] are synthesized, first, by inserting the Ru-CO fragment into porphyrins. The resulting precursor ruthenium(II) carbonyl porphyrin complex, often formulated as (por)Ru(CO), possesses a weakly coordinated solvent molecule *trans* to CO. The solvent molecule

✉ Dennis Awasabisah
dawasabi@fitchburgstate.edu

[1] Biology and Chemistry Department, Fitchburg State University, 160 Pearl St, Fitchburg, MA 01420, USA

[2] Department of Chemistry and Biochemistry, Stephenson Life Science Research Center, University of Oklahoma, 101 Stephenson Parkway, Norman, OK 73019, USA

[3] Gustaf H. Carlson School of Chemistry, Arthur M. Sackler Sciences Center, 950 Main Street, Worcester, MA 01610, USA

in the resulting (por)Ru(CO)(solvent), which is introduced during workup, can be replaced by stronger π-donor and/or σ-donor ligands. For example, the six-coordinate ruthenium porphyrin carbonyls, (OEP)Ru(CO)(py) and (OEP)Ru(CO)(Im) have been prepared by this method [20]. We were interested in expanding the study on the reaction of (por)Ru(CO) with quinoline-based ligands. To this end, we have prepared the ruthenium(II) porphyrin complex, (OEP)Ru(CO) (OEP = 2,3,7,8,12,13,17,18-octaethylporphyrinato dianion) as a synthetic heme active site and studied its reactivity with quinine (QN) in forming the (OEP)Ru(CO)(QN) adduct. We have examined the site of binding of the QN ligand to the ruthenium center (OEP)Ru(CO) by comparing the spectroscopic properties of the adducts formed between (OEP)Ru(CO) and quinoline (Qnl) (Fig. 1). We have obtained the X-ray crystal of (OEP)Ru(CO)(Qnl) to assist in understanding the site of binding of the quinoline-based drugs with the Ru center. We have also studied the redox behaviors of the (OEP)Ru(CO)(Q) adducts.

Experimental section

General procedures

Unless otherwise stated, all reactions and manipulations were performed under an atmosphere of nitrogen using standard Schlenk glassware. Reagents were purchased from commercial sources (see below) and used as received, except noted otherwise. Dichloromethane and n-hexane were deaerated by a three-cycle freeze–pump–thaw and dried over a 4 Å molecular sieves before use.

The free-base porphyrin, 2,3,7,8,12,13,17,18-Octaethyl-21*H*,23*H*-porphine [$(OEP)H_2$, 97%], triruthenium dodecacarbonyl [$Ru_3(CO)_{12}$, 99%], decalin (≥ 99%), dichloromethane (CH_2Cl_2, ≥ 99.8%), n-hexane (95%), quinine (QN, 98%), tetrabutylammonium hexafluorophosphate (NBu_4PF_6, ≥ 99%) and ferrocene (Fc, 98%) were purchased from Sigma-Aldrich. Quinoline (Qnl, 99%) and Chloroform-*d* ($CDCl_3$, 99.8 atom %D, 1 v/v% TMS) were purchased from Thermo Fisher Scientific.

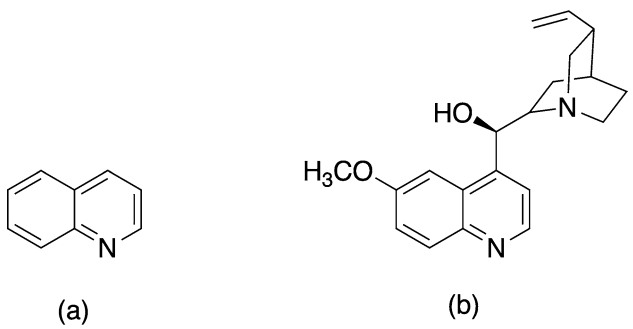

Fig. 1 Structures of the ligands used in this work: **a** quinoline; **b** Quinine

Infrared spectra were collected at room temperature on a Perkin-Elmer Spectrum 65 FT-IR Spectrophotometer equipped with ATR accessory. The ^1H NMR spectra were obtained on a Varian Mercury 400 MHz spectrometer at 25 °C and the signals were referenced to the residual signal of the solvent employed ($CHCl_3$ at 7.26 ppm). Coupling constants are reported in Hz. UV–Visible spectra were collected on a Thermo Scientific Evolution 201 UV–Visible Spectrophotometer.

ESI mass spectra were obtained on a Micromass Q-TOF mass spectrometer. Elemental analyses were obtained by staff of Atlantic Microlab, Norcross, GA. X-ray diffraction data were collected using a D8 Quest κ-geometry diffractometer with a Bruker Photon II cmos area detector [21, 22] and an Incoatec I μ s microfocus Mo Kα radiation (λ = 0.71073 Å). Cyclic voltammetry measurements were performed using a Gamry Interface 1000B Potentiostat/Galvanostat/ZRA. In all the electrochemical experiments, a three-electrode cell was utilized and consisted of a 3.0 mm diameter Pt disk working electrode, a Pt wire counter electrode, and a Ag/AgCl wire as reference electrode. Solutions were deaerated before use by passing a stream of N_2 gas through the solution for a minimum of 10 min. A blanket of N_2 was maintained over the solution while performing the experiments. The electrochemical experiments were performed in solutions containing 0.1 M NBu_4PF_6 and 1.0 mM of the analyte. Ferrocene, Fc (1.0 mM) was used as internal standard for the electrochemical experiments and potentials were referenced to the Fc/Fc^+ couple at 0.00 V.

Synthesis of compounds

Synthesis of (OEP)Ru(CO) (1)

The compound, (OEP)Ru(CO) (**1**) was prepared by a slight modification of the method reported in the literature [23]. In this work, the free-base porphyrin, $(OEP)H_2$ (503.9 mg, 0.942 mmol) and $Ru_3(CO)_{12}$ (613.6 mg, 0.960 mmol) were refluxed in decalin (100 mL) for 4 h. The resulting dark-red solution was concentrated, then purified by column chromatography (alumina) using 100% dichloromethane to a 2:1 dichloromethane/acetone solvent gradient as eluent. The product was crystallized from n-hexane and dried *in vacuo* to give a bright-red precipitate characterized as **1** (583.0 mg, 93% isolated yield). IR (ATR, cm^{-1}): $\upsilon_{CO} = 1918$ (vs), 1922 (s) (in CH_2Cl_2). Also: 2966 (m), 2930 (m), 2867 (m), 1683 (w), 1590 (m), 1539 (w), 1464 (m), 1447 (m), 1375 (m), 1319 (w), 1272 (s), 1227 (m), 1144 (m), 1110 (m), 1056 (m), 1017 (s), 991 (m), 962 (s), 922 (w), 840 (s), 745 (s), 712 (m). ^1H NMR ($CDCl_3$, 400 MHz): δ (ppm) 9.96 (*s*, 4 H, *pyrrole-H* of OEP), 4.04 (*q*, *J* = 7.7 Hz, 16 H, CH_2),

1.94 (*t*, *J* = 7.6 Hz, 24 H, *CH*$_3$). UV–vis: (CH_2Cl_2):λ_{max}, nm (log ε) 392 (4.80) Soret, 547 (4.02), 515 (3.65), 302 (3.71), 246 (3.80). Suitable crystals for X-ray crystallography were obtained by slow evaporation of a CH_2Cl_2/n-hexane (2:1) solution of **1** and were characterized as the six-coordinate monohydrate complex, (OEP)Ru(CO)(H_2O).

Preparation of (OEP)Ru(CO)(Qnl) (2)

A 50 mL Schlenk tube equipped with a magnetic stir bar was charged with **1** (101 mg, 0.153 mmol) and CH_2Cl_2 (10 mL). The mixture was stirred at room temperature, under N_2 atmosphere resulting in a red solution. An excess amount of quinoline (90 µL, 0.746 mmol) was added to the solution and stirred for 48 h. During this period, the solution changed color from red to dark-magenta. After 48 h of stirring, the resulting solution was slowly reduced *in vacuo* to approximately 3 mL. n-Hexane (10 mL) was then added. The solvent was slowly removed under reduced pressure, and the resulting solid was carefully washed with cold n-hexane (3 mL). The product was dried *in vacuo* to give a red precipitate that was characterized as **2** (99.8 mg, 83% isolated yield). IR (ATR, cm^{-1}): υ_{CO} = 1938 (vs), 1932 (s) (in CH_2Cl_2). Also: 2964 (m), 2930 (m), 2868 (m), 1896 (w), 1634 (w), 1599 (w), 1536 (w), 1510 (w), 1464 (m), 1371 (m), 1316 (w), 1271 (m), 1230 (m), 1147 (m), 1109 (m), 1056 (m), 1017 (s), 991 (m), 959 (s), 860 (w), 838 (m), 800 (m), 783 (m), 746 (m), 711 (m). ^{1}H NMR ($CDCl_3$, 400 MHz): δ (ppm) 9.92 (*s*, 4 H, *pyrrole-H)*, 7.76 (*d*, *J* = 8.6 Hz, 1 H, *Qnl-H*), 7.49 (*app d*, *J* = 7.7 Hz, 1 H, *Qnl-H*), 7.35 (*app d*, *J* = 6.9 Hz, 1 H, *Qnl-H*), 7.32 (*app d*, *J* = 4.9 Hz, 1 H, *Qnl-H*), 7.28 (*app d, J* = 6.5 Hz, 1 H, *Qnl-H* H), 6.86 (*app d*, *J* = 4.8 Hz, 1 H, *Qnl-H*), 6.25 (*br s*, 1 H, *Qnl-H*), 4.01 (*dq*, *J* = 7.7 Hz, 3.1 Hz, 16 H, CH_3CH_2), 1.92 (*t*, *J* = 7.7 Hz, 24 H, CH_3CH_2). UV–Vis: (CH_2Cl_2): λ_{max}, nm (log ε) 392 (5.34) Soret, 547 (4.51), 515 (4.18), 314 (4.32), 302 (4.32), 229 sh (4.71), 227 (4.73). ESI mass spectrum (TOF), *m/z*: 833.2400 for $[M + MeCN + H]^+$; 764.1798 for $[M - CO + H]^+$; 741.1968 for $[M - Qnl + DMSO + H]^+$. Anal. Calcd. for $C_{46}H_{51}N_5ORu \bullet 0.5H_2O$: C, 69.06; H, 6.55; N, 8.75. Found: C, 68.92; H, 6.63; N, 8.37. Suitable crystals for X-ray crystallography were obtained by slow evaporation of a CH_2Cl_2/ n-hexane solution of the compound at room temperature and characterized as structure **2A**. In a separate crystallization process, a second batch of single crystals were obtained and were determined to be the same structure as 2A, but with quite different parameters (vide infra). We refer to this second crystal structure as **2B**.

Preparation of (OEP)Ru(CO)(QN) (3)

A 50 mL Schlenk tube equipped with a magnetic stir bar was charged with **1** (50.2 mg, 0.0758 mmol) followed by CH_2Cl_2 (10 mL). The solution was stirred under N_2 atmosphere resulting in a red solution. The red solution was treated with a slight excess of quinine, QN (40.1 mg, 0.123 mmol) and the solution was allowed to stir for 48 h. After 48 h, the resulting dark-red solution was slowly reduced to 3 mL under vacuum. n-Hexane (10 mL) was added and the mixture was stirred vigorously for 1 min. After several hours of sitting undisturbed, precipitates began to form. The supernatant was discarded. The red precipitate was washed twice (two 5 mL portions) with n-hexane, and the supernatant discarded each time. The precipitate was dried under vacuum to give a red solid characterized as **3** (52.4 mg, 70% isolated yield). IR (ATR, cm^{-1}): 1931 (vs), 1930 (s) (in CH_2Cl_2). Also, 3152 br (w), 2963 (m), 2930 (m), 2870 (m), 1688 (w), 1623 (m), 1591 (w), 1510 (m), 1467 (m), 1451 (m), 1431 (m), 1374 (m), 1272 (m), 1241 (m), 1229 (m), 1150 (m), 1108 (m), 1056 (m), 1032 (w), 1019 (s), 992 (m), 960 (m), 919 (w), 840 (m), 744 (m), 717 (m), 647 (m). ^{1}H NMR ($CDCl_3$, 400 MHz): δ (ppm) 9.81 (*s*, 4 H, *pyrrole-H*), 7.10 (*dd*, *J* = 6.2 Hz, *J* = 3.2 Hz, 2 H, *qnl-H*), 6.60 (*br s*, 1 H, *qnl-H*), 5.89 (*br s*, 1 H, *qnl-H*), 5.36 (*m*, *J* = 8.0 Hz, 1 H, $CH=CH_2$), 4.76 (*overlapping d*, *J* = 10.8 Hz, 2 H, $CH_2=CH$), 4.70 (*s*, 1 H, CH(OH)), 4.26 (*br s*, 1 H *qnl-H*), 3.92 (*app q*, *J* = 6.7 Hz, 16 H, CH_2CH_3), 3.23 (*s*, 3 H, OCH_3), 1.84 (*t*, *J* = 7.6 Hz, 24 H, CH_3CH_2), 2.26 – 1.26 (overlapping *m*, 11 H, *quinuclidine-H's*). UV–Vis (CH_2Cl_2): λ_{max}, nm (log ε) 392 (5.11) Soret, 547 (4.28), 515 (3.95), 331 (4.19), 320 (4.19), 232 (4.64), 227 (4.59). ESI mass spectrum (TOF), *m/z*: 1333.5198 for $[M + QN + Na]^+$; 663.2582 for $[M - QN + H]^+$; 325.1913 for $[QN + H]^+$. Anal. Calc. for $C_{56}H_{68}N_6O_3Ru \bullet 0.5H_2O$: C, 68.79; H, 6.99; N, 8.44 Found: C, 68.96; H, 7.08; N, 8.08.

X-ray crystallography

A red plate-shaped crystal of **1** and of dimensions 0.110 × 0.172 × 0.202 mm was selected for structural analysis. Intensity data for this compound were collected using a D8 Quest κ geometry diffractometer with a Bruker Photon II cmos area detector [21, 22] and an Incoatec Iμs microfocus Mo Kα source (λ = 0.71073 Å). The sample was cooled to 100(2) K. Cell parameters were determined from a least-squares fit of 9810 peaks in the range 2.81 < θ < 31.55°. A total of 107,368 data were measured in the range 2.304 < θ < 31.585° using φ and ω oscillation frames. The data were corrected for absorption by the empirical method [24] giving minimum and maximum transmission factors of 0.5989 and 0.6482. The data were merged to form a set of 10,990 independent data with R(int) = 0.0320 and a coverage of 99.7%.

The triclinic space group *P*1 was determined by statistical tests and verified by subsequent refinement. The structure was solved by dual-space methods and refined by full-matrix

least-squares methods on F^2 [25, 26]. The positions of hydrogens bonded to carbons were initially determined by geometry and were refined using a riding model. Hydrogens bonded to O2 were located on a difference map, and their positions were refined with a riding model. Non-hydrogen atoms were refined with anisotropic displacement parameters. Hydrogen atom displacement parameters were set to 1.2 times the isotropic equivalent displacement parameters of the bonded atoms. A total of 397 parameters were refined against 10,990 data to give $wR(F^2) = 0.0634$ and $S = 1.004$ for weights of $w = 1/[\sigma^2 (F^2) + (0.0300\ P)^2 + 1.4000\ P]$, where $P = [F_o^2 + 2F_c^2] / 3$. The final $R(F)$ was 0.0232 for the 10,374 observed, $[F > 4\sigma(F)]$, data. The largest shift/s.u. was 0.002 in the final refinement cycle. The final difference map had maxima and minima of 1.239 and -0.692 e/Å^3, respectively. Structural diagrams were prepared using Mercury 2021.3.0 program [27]. A summary of the crystal and structure refinement data is shown in Table 1.

A red block-shaped crystal, **2A** of dimensions $0.074 \times 0.126 \times 0.264$ mm was selected for structural analysis. Intensity data for this compound were collected and the structure solved as described for 1 (Table 1). Crystal structure **2B** with monoclinic space group $P2_1/n$ was determined similarly as indicated by the crystal data and structure refinement data in Table 1.

Results and discussion

Preparation, spectroscopy and X-ray crystallography

The ruthenium(II) porphyrin complexes, (OEP)Ru(CO)(Q) (Q = Qnl (**2**) and QN (**3**)) were prepared by reacting a dichloromethane solution of (OEP)Ru(CO) (**1**) with quinoline (Qnl) and quinine (QN), respectively (Scheme 1). The reactions occurred at room temperature over a 24 – 48 h period, producing red solids at 70 – 83% isolated yields. The compounds are air-stable as solids at room temperature, and showed no evidence of decomposition over several days as judged by IR and ^{1}H NMR spectroscopy.

Table 1 Crystal data and structure refinement for 1, 2A and 2B

	1	2A	2B
Temperature, K	100(2)	100(2)	100(2)
Crystal system	triclinic	monoclinic	monoclinic
Space group	$P\bar{1}$	$P2_1/n$	$P2_1/n$
Crystal dimensions, mm	0.11 × 0.17 × 0.20	0.07 × 0.13 × 0.26	0.03 × 0.06 × 0.22
Unit cell dimensions			
a, Å	10.1174(3)	9.3130(5)	14.1296(16)
b, Å	13.6140(5)	12.8571(6)	15.2253(14)
c, Å	13.8415(5)	32.5804(18)	19.530(3)
α, °	65.2499(11)	90	90
b, °	75.8287(11)	95.0171(16)	111.017(4)
γ, °	89.8541(12)	90	90
Volume, Å^3	1667.84(10)	3886.2(4)	3921.9(8)
Z, Z'	2, 1	4, 1	4, 1
Density Mg/m^3	1.354	1.352	1.340
Absorption coefficient, mm^{-1}	0.508	0.446	0.442
Max. and min. transmission	0.6482 and 0.5989	0.6469 and 0.6187	0.5628 and 0.5095
θ range for data collection, °	2.304 to 31.585	2.335 to 27.952	2.207 to 27.265
h k l ranges	$-14 \le h \le 14$	$-12 \le h \le 12$	$-18 \le h \le 18$
	$-20 \le k \le 20$	$-16 \le k \le 16$	$-19 \le k \le 19$
	$-20 \le l \le 20$	$-42 \le l \le 42$	$-25 \le l \le 25$
Reflections collected	107,368	81,610	150,036
Independent reflections	10,990 [R(int) = 0.0320]	9279 [R(int) = 0.0254]	8714 [R(int) = 0.0787]
Data/restraints/parameters	10,990 / 0 / 397	9279 / 0 / 478	8714 / 1357 / 727
$wR(F^2$ all data)	$wR_2 = 0.0634$	$wR_2 = 0.0677$	$wR_2 = 0.1738$
R (F obsd data)	$R_1 = 0.0232$	$R_1 = 0.0263$	$R_1 = 0.0593$
Goodness-of-fit on F^2	1.004	1.009	1.001
Observed data [I > 2σ(I)]	10,374	8736	6285
Largest and mean shift / s.u	0.002 and 0.000	0.002 and 0.000	0.002 and 0.000
Largest diff. peak and hole, e/Å^3	1.239 and -0.692	1.133 and -0.976	0.949 and -0.944

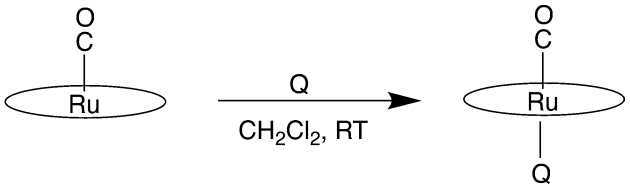

Scheme 1 Synthesis of (OEP)Ru(CO)(Q) [Q = Quinoline, Qnl (2); QN (3)] from (OEP)Ru(CO) (1)

Table 2 The υ_{NO} bands of the compounds **1** – **3**

Compound	ATR υ_{CO} (cm^{-1}) Solid	ATR, υ_{CO} (cm^{-1}) CH_2Cl_2
1	1918	1922
2	1938	1932
3	1931	1930

Compounds **1** – **3** were characterized by IR spectroscopy both in the solid form and in CH_2Cl_2. Table 2 lists the υ_{CO} bands for compounds **1** – **3**. These IR bands are in the range of the υ_{CO} of ruthenium(II) carbonyls. For example, solid samples of compound **2** have a strong υ_{CO} band at 1938 cm^{-1}, which is in the same range as those of other *N*-bound complexes, (OEP)Ru(CO)(t-Bu(py)) (υ_{CO} = 1935 cm^{-1}) [28], (OEP)Ru(CO)(py) and (OEP)Ru(CO)(Im) (υ_{CO} = 1933 cm^{-1}) [20], but higher (by 20 cm^{-1}) than that of the precursor complex, **1**. Similarly, a CH_2Cl_2 solution of **2** displayed υ_{CO} bands at 1932 cm^{-1} in the IR spectrum. Thus, in **2**, based on the IR spectral data, Qnl is coordinated to the axial position of the ruthenium(II) center through the quinoline-N.

The υ_{CO} band in **3** was observed at 1931 cm^{-1}, which is 13 cm^{-1} higher than that of the precursor compound **1**. This υ_{CO} band is in the same range as that of **2**, and is an indication that the site of binding is though the quinoline-N, and not the other basic sites (i.e., hydroxyl group, the quinuclidine-N, or the olefin). The υ_{CO} band in **3** is, as expected, lower than that of **2**. This parallels the stronger donor effect of quinine compared to quinoline. Quinine donates more electron density for backdonation into the RuCO moiety. The IR spectrum of **3** also displays medium intensity peaks at 1623, 1510, 1431, and 1241 cm^{-1} due to vibrations related to the QN ligand. The proposed binding sites of the ligands to Ru in compounds **2** and **3** are supported by ^{1}H NMR data (*vide infra*).

The ^{1}H NMR spectrum of **1** showed only the expected peaks for the OEP porphyrin. Even as solids, ruthenium(II) porphyrin carbonyls such as (TPP)Ru(CO), and possibly **1** could easily pick up a water molecule if they are exposed to air [29]. Indeed, the X-ray crystal structure of **1** (*vide infra*) revealed H_2O is coordinated to Ru, although there were no peaks associated with H_2O in its ^{1}H NMR spectrum. The ^{1}H NMR spectroscopic data for compounds **1**–**3** revealed the peaks associated with the porphyrin macrocycle. The porphyrin *pyrrole-H* peaks were observed at 9.96, 9.92 and 9.81 for **1**, **2** and **3**, respectively. Similarly, the peaks associated with the ethyl groups, CH_3CH_2 were displayed at the expected chemical shifts of ~ 4.0 (CH_2) and ~ 1.9 (CH_3).

In addition to the signals due to the OEP macrocycle, the ^{1}H NMR spectra of compounds **2** and **3** displayed new peaks associated with the Q ligands. As expected, the associated Q proton peaks are shifted upfield due to ring current effect from the OEP macrocycle [30]. For example, the ^{1}H NMR peaks for the bound Qnl in compound **2** appeared at δ 7.76 *d* (1 H), 7.49 *app d* (1 H), 7.35 *app d* (1 H), 7.32 *app d* (1H), 7.28 *app d* (1 H), 6.85 *d* (1 H) and 6.25 br *s* (1 H). The ^{1}H NMR spectrum for the uncoordinated free-base Qnl ligand collected at similar experimental conditions and in the same solvent displayed the following peaks: δ 8.90 *dd* (1 H), 8.11 *dd* (1 H), 8.10 *d* (1 H), 7.78 *d* (1 H), 7.71 – 7.67 *dddd* (1 H), 7.53–7.50 *dddd* (1 H), 7.36 *dd* (1 H). Similar upfield δ shifts of ligand peaks have been recorded in (OEP)Ru(CO)(py) [20] and (OEP)Ru(CO)(Im) [28], as well as in *O*-bound six-coordinate ruthenium nitrosyl porphyrins [17, 18].

We then turned our attention to understanding the site of binding of QN to ruthenium in **3**. Since the hydroxyl group, the quinuclidine N, the quinoline N and the olefin are possible sites of binding, we examined the effects of the ring current on the chemical shifts of the various protons in QN via the ^{1}H NMR spectrum of **3**. We anticipated that this information would help us determine the site of binding of QN in **3** in solution. The ^{1}H NMR of **3** displayed new peaks associated with QN ligand and were observed more upfield relative to the free-base QN. The ^{1}H NMR signals of the quinoline moiety in **3** were observed at 7.10 *dd* (2 H), 6.60 *br s* (1 H), 5.89 *br s* (1 H), 4.26 *br s* (1 H). Other QN signals were observed at 5.36 m (1 H) and 4.76 *app d* (2 H), and were assigned to the vinyl-*H* on the quinuclidine ring. The respective vinyl-*H* signals in the free-base QN ligand are 5.78 m (1 H) and 4.95 *app d* (2H). We note that the quinoline-*H*'s in **3** experienced the largest upfield δ shifts suggesting that the quinoline group is probably closest to the Ru center, and as a result experienced the largest effect of the porphyrin ring current. The proposed site of binding of QN is also supported by the fact that the H's on the quinuclidine ring did not shift as much as those of the quinoline moiety. Signals due to the quinuclidine ring in **3** were observed as several overlapping multiplets between δ 2.26 and 1.26, thus, supporting binding of Ru through the quinoline N.

The UV–visible spectra of compounds **1 – 3** collected in dichloromethane revealed the expected Soret band at 392 nm, which is due to porphyrin $a_{1u}(\pi)$–$e_g^*(\pi)$ transitions. Additionally, the characteristic α and β bands (Q bands)

attributed to $a_{2u}(\pi)$–$e_g^*(\pi)$ transitions were recorded at 547 and 515 nm, respectively [31]. There are however, distinguishing characteristic bands in the 220 – 350 nm region depending on the sixth ligand on the (OEP)Ru(CO) unit (Fig. 2). For example, the following peaks were observed in **3**: 331, 320, 232 and 232 nm, and are associated with the quinine ligand [32]. In the quinoline complex, **2** bands at 314, 302, 229 (sh), and 227 nm were recorded and these were similarly associated with the Qnl ligand. Hence, UV–visible spectra of the compounds parallels the observed UV–visible spectrum of (OEP)Ru(CO)(Py) recorded in a similar solvent [33]. The UV–visible spectra of **2** and **3** both point to the presence of a quinoline functionality.

In order to gain insight into the solid-state structures of these complexes, we resorted to X-ray crystallography analysis of single crystal samples of **1** and **2**. We obtained two crystal structures of **2** (**2A** and **2B**) from different crystallization batches. Structures **2A** and **2B** have quite different cell parameters and the relative orientations of the ethyl groups relative to the porphyrin ring are different for these two compounds. The molecular structure of compound **2A** is shown in Fig. 3a and that of **2B** is shown in Fig. S6 (supplementary material). Selected bond lengths and angles of **2A**, **2B** and **1** are listed in Table 3.

As shown in Fig. 3, compound **2A** is a six-coordinate ruthenium(II) porphyrin complex with a Qnl ligand and CO at the axial positions of the porphyrin macrocycle. The Qnl ligand is bound to Ru via its nitrogen atom. The Ru atom is displaced by only 0.06 Å from the 24-atom mean plane towards the Qnl ligand. The Qnl ligand plane is essentially perpendicular to the 24-mean plane of the porphyrin macrocycle with the angle between the two planes being 81.89°. In the crystal packing of **2A**, the two Qnl groups of adjacent porphyrins have parallel-displaced configurations. The two Qnl planes are separated by 3.30 Å suggesting a relatively

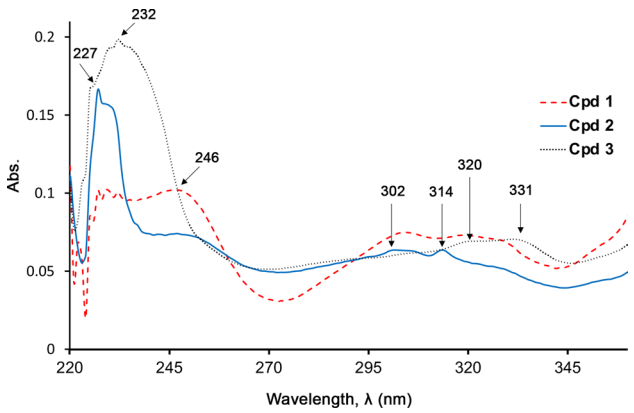

Fig. 2 UV–visible spectra of compounds 1 (2.39×10^{-5} M), 2 (3.06×10^{-6} M) and 3 (4.51×10^{-6} M) collected in CH_2Cl_2 at room temperature. Showing signals in the 220 – 350 nm wavelength range. See full spectrum in the S12

strong π -π interaction between the two quinoline ligands and mimics the interlayer structure of graphite [34]. These two adjacent porphyrins have a mean plane separation of 9.29 Å, and their relative positioning are laterally shifted at 3.55 Å (Fig. 3b). The porphyrin macrocycle is mildly ruffled with the ring slightly out-of-plane from the 24-mean porphyrin plane and specifically away from the Qnl ring (Fig. 4a,b).

Similarly, in the X-ray crystal structure of **2B** the mean quinoline group plane is perpendicular to the 24-mean porphyrin plane at an angle of 82.05° (Fig. S8). The Ru atom is displaced by only 0.020 Å towards the Qnl ligand. In the crystal packing diagram, the two closest adjacent porphyrins have a mean plane separation of 3.79 Å and they are oriented head-to-head at the CO ends. As a result, their relative lateral shift is 7.06 Å, more than twice that of **2A**. We note the porphyrin macrocycle in **2B** is similarly mildly ruffled (Fig. S9b) and that several parts of **2B** were disordered. This disorder is likely associated with small amounts of isoquinoline in the quinoline reagent that co-crystallized with quinoline in the crystallization of **2**. We detected ~ 0.6% (by ^{1} HNMR spectroscopy) of isoquinoline in the quinoline sample used for the analysis. We plan to study the isoquinoline porphyrin complex in future work.

The Ru–N_{axial}(N_{axial} = quinoline N) bond distances in **2A** is 2.3408(13) Å, which is longer than its average Ru–N_p bond distance of 2.0574(12) Å and 2.055(3) Å, respectively. The Ru–N_{axial} bond distances are also longer than those recorded in (OEP)Ru(CO)(Im) (2.192(4) Å) [35], (OEP)Ru(CO)(Py) (2.239(2) Å) [36], and (OEP)Ru(py)$_2$ (2.100 Å) [37], thus, reflecting the *trans influence* of CO on the lower *trans effect* axial ligands, Qnl, Im and Py respectively. The Ru–CO bond distance in **2A** recorded as 1.8081(15) Å is shorter than that in (OEP)Ru(CO)(Im) (1.829(5) Å, but comparable to that of (OEP)Ru(CO)(Py) (1.812(6) Å). The C–O bond length in **2A** is 1.155(2) Å and is similarly comparable to those of (OEP)Ru(CO)(Im) (1.156(5) Å) and (OEP)Ru(CO)(Py) (1.158(6) Å). The ∠Ru–C–O angle in **2A** is essentially linear, as is the case for (OEP)Ru(CO)(Im) and (OEP)Ru(CO)(Py), but we note that the ∠Ru–C–O in **2A** (176.51(14)°) is slightly lower than that of **2B** (179.0(4)°).

The X-ray diffraction studies of a single crystal sample of **1** revealed the monohydrate complex, (OEP)Ru(CO)(H_2O) (Fig. 5a). The average Ru–N_p bond lengths in **1** is 2.0554(9) Å and is within range of those of other ruthenium(II) porphyrin carbonyl complexes. We note that in **1** because one water hydrogen (H2B) forms a hydrogen bond to a symmetry-related water oxygen, the occupancy of H2B was set to 0.5. The water hydrogen H2C was also assigned an occupancy of 0.5 to give the water the correct number of hydrogens.

The Ru–O bond distance in **1** is 2.248(3) Å and it compares quite well with the 2.242 Å recorded in both (OEP)Ru(CO)(EtOH)[36] and (OEP)Ru(CO)(THF) [38], but quite

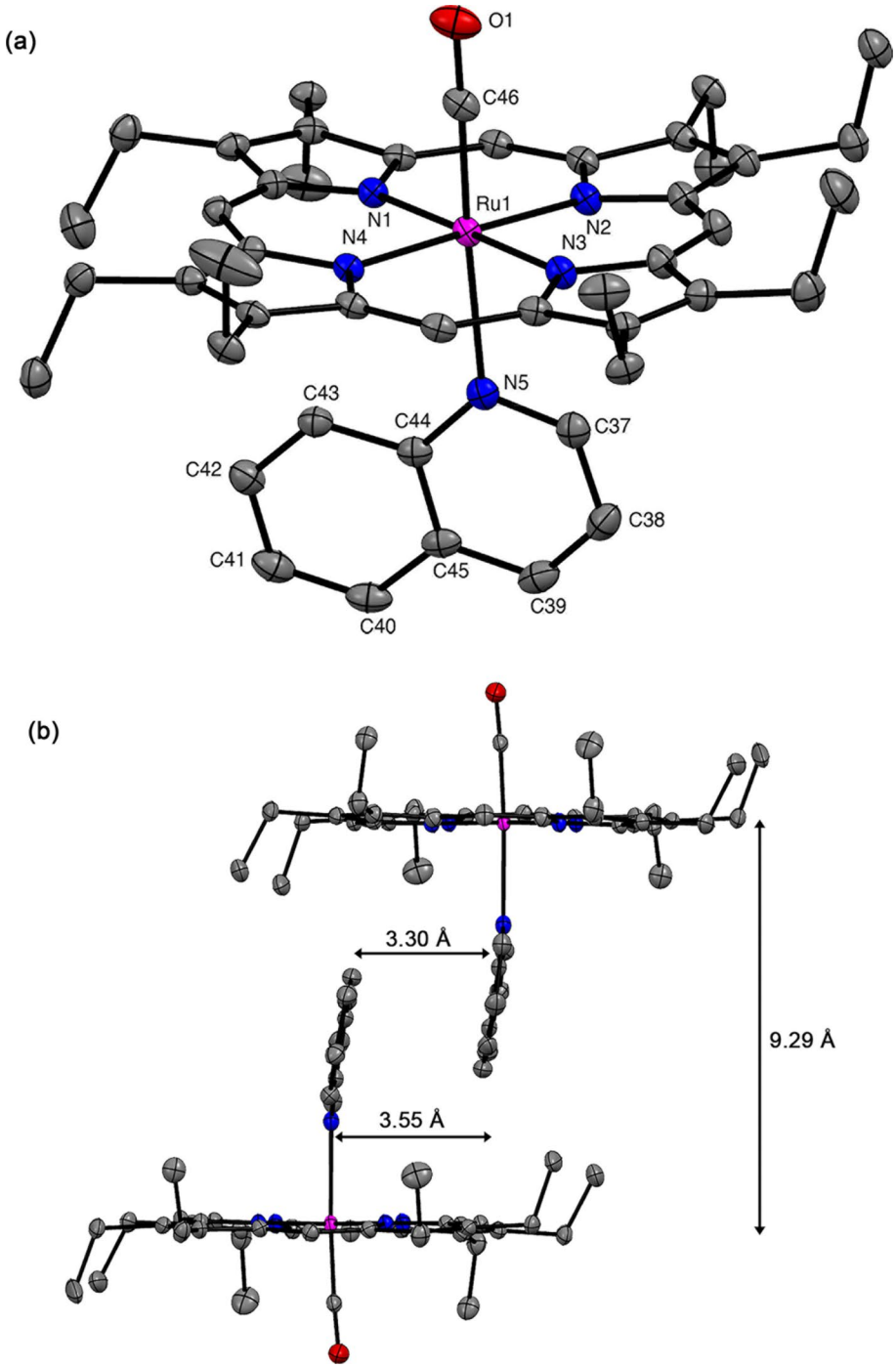

Fig. 3 **a** Molecular structure of **2A** **b** Relative positions of adjacent porphyrin macrocycles in the crystal structure of **2A**. Hydrogen atoms have been omitted for clarity

longer than the aryloxide Ru – OC_6H_4-*p*-Me (1.964(11) Å) and Ru – O(Ru) (1.1789(11) Å) bond distances in [(TPP)Ru(OC_6H_4-*p*-CH_3)]$_2$O [39]. The ∠Ru–C–O of **1** is essentially linear with bond angle of 178.12(11) Å.

The porphyrin mean plane of separation between two adjacent porphyrins in **1** is 5.17 Å, and shows the molecules are substantially closer in **1** than in **2**, which is expected due to the bulkier Qnl ligand in **2**. A lateral shift of 3.65 Å between two adjacent porphyrins was determined for **1**. We note that the Ru atom in 1 is displaced by 0.15 Å from the 24-atom mean porphyrin plane towards the CO ligand, but was displaced in the opposite direction in **2**. Efforts to grow suitable single crystals for X-ray crystallography of **3** were unsuccessful, instead precipitates were obtained. The precipitates had similar spectral features as before suggesting **3** is stable in solution under N_2 over several days.

Compounds **2** and **3** were also characterized by mass spectrometry. The MS-TOF data for **2** showed peaks at

Table 3 Selected bond lengths (Å) and bond angles (°) of **1**, **2A** and **2B**

	1	**2A**	2B
C–O	1.1567(15)	1.155(2)	1.158(6)
Ru–N_p, Avg	2.0554(9)	2.0574(12)	2.055(3)
Ru–C(O)	1.8014(12)	1.8081(15)	1.812(6)
Ru–N_q	–	2.3408(13)	2.352(7)
Ru–O	2.2477(9)	–	–
∠Ru–C–O	178.12(11)	176.51(14)	179.0(4)

m/z 833.2400, 764.1798 and 741.1968 and assigned to $[(OEP)Ru(CO)(Qnl) + MeCN + H]^+$, $[(OEP)Ru(Qnl) + H]^+$ and $[(OEP)Ru(CO) + DMSO + H]^+$, respectively. The MS data for **3** displayed peaks at m/z 890.2352 $[(OEP)Ru(CO)(8\text{-}HOQ) + 2MeCN + H]^+$ and 741.1964 $[(OEP)Ru(CO) + DMSO + H]^+$. The quinine complex, **3** displayed peaks at *m/z* 1333.5198 assigned to $[M + QN + Na]^+$.

Cyclic voltammetry

The redox behavior of compounds **1 – 3** were investigated by cyclic voltammetry in an anhydrous dichloromethane solution containing NBu_4PF_6 as support electrolyte. The electrochemical cell was composed of Pt working electrode, Ag/AgCl reference electrode and a Pt wire auxiliary electrode.

We begin by examining the redox behaviors of compounds **2**. The cyclic voltammogram of reveals that **2** undergoes a reversible one-electron first oxidation at $E^{o'} = +0.21$ V vs. Fc/Fc^+ couple (Fig. 6a). Compound **3** similarly undergoes a reversible first oxidation at + 0.19 V vs. Fc/Fc^+ couple (Fig. 6b). Oxidation potentials in this range are associated with porphyrin centered oxidations [40]. Thus, the π-radical cations $[2]^{\bullet+}$ and $[3]^{\bullet+}$, respectively are generated after first oxidation of **2** and **3**.

We note that the cathodic-to-anodic current peak ratios (i_{pc}/i_{pa} was determined to be ~ 1.0 and the plots of the i_{pa} *vs* square root of the scan rate ($\upsilon^{1/2}$) for the first oxidations of compounds **2** and **3** show a linear relationship, thus, suggesting a diffusion-control redox process. The peak separations, $\Delta E_p = |E_{pa} - E_{pc}|$ in peak potentials for the first oxidations each of compounds **2** (62 mV) and **3** (141 mV) at a scan rate of 200 mVs^{-1} are near equivalent to that of their respective Fc/Fc^+ internal standard values of 62 mV and 148 mV, indicating that the first oxidations are single-electron reversible electron-transfer processes.

We note that the second oxidation of **2** is reversible and occurs at $E^{o'} = +0.74$ V. Similarly, the ΔE_p values of the second oxidation of **2** is identical to that of the Fc/Fc^+ couple, also suggesting a reversible one-electron transfer process. The second oxidation of **3**, however, is irreversible and occurs at an anodic peak potential, $E_{pa} = +0.66$ V and the cathodic peak potential, E_{pc} being + 0.74 V. In addition, there was a pre-wave after the first oxidation of **3** which occurred at $E_{pa} = +0.62$ V. Table 4 summarizes the redox potentials of the compounds referenced with Fc/Fc^+ couple as internal standard.

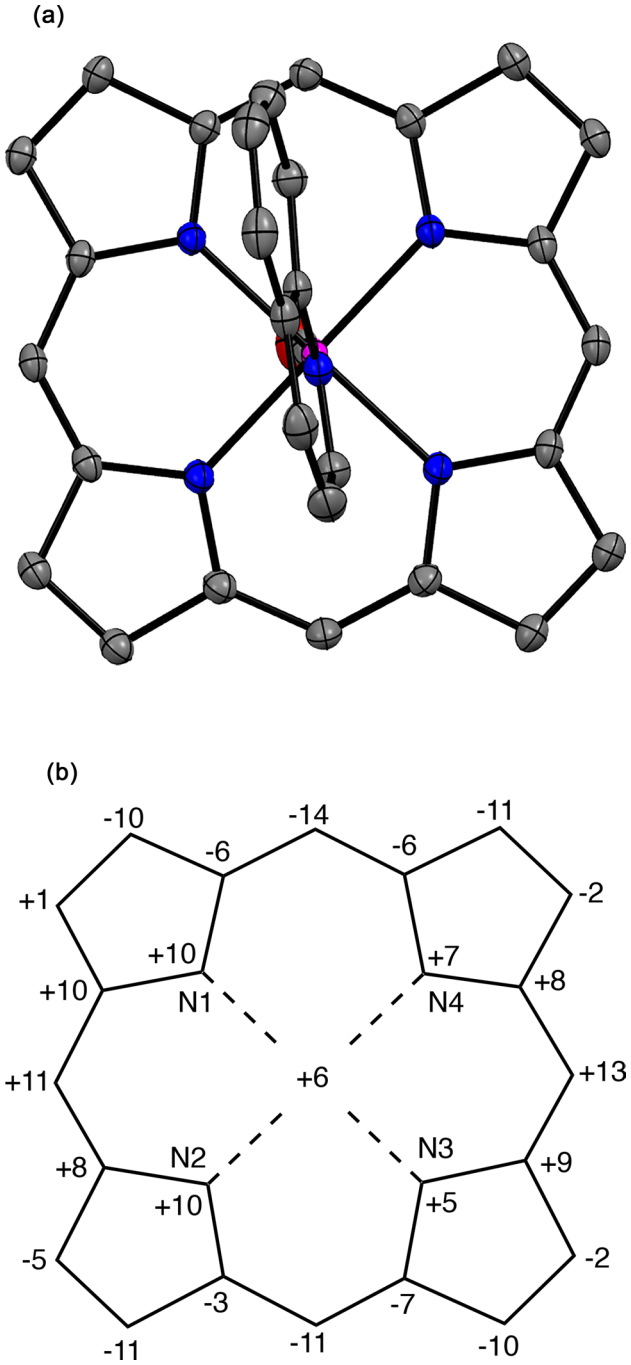

Fig. 4 **a** Molecular structure of **2A** viewing from the Qnl ligand perpendicular to the 24-mean porphyrin plan. Hydrogen atoms have been omitted for clarity **b**: Perpendicular atom displacements (in Å ~ 100) of the porphyrin core from the porphyrin 24-atom mean plane

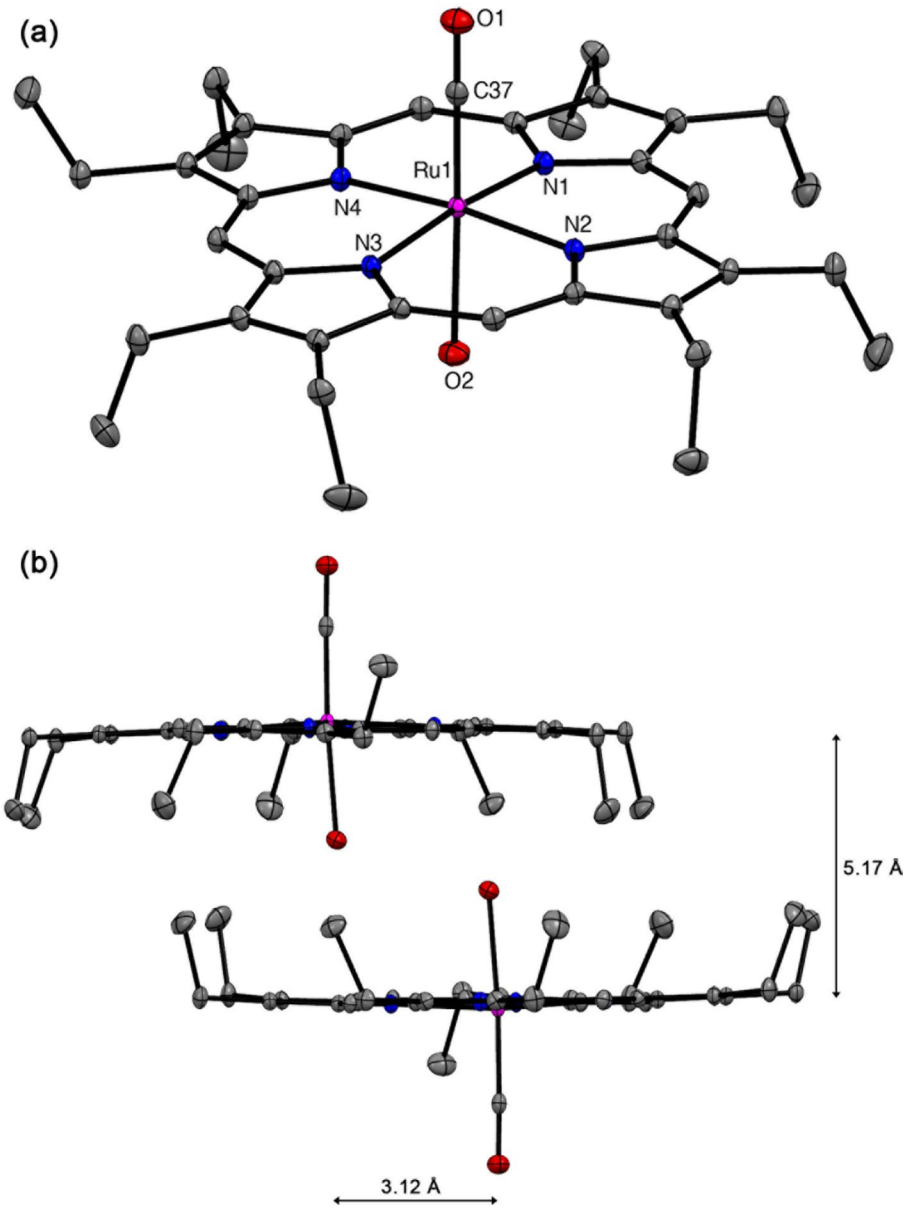

Fig. 5 **a** Molecular structure of **1** as a monohydrate complex. **b** Relative positions of adjacent porphyrin macrocycles in the crystal structure of **1**. Hydrogen atoms have been omitted for clarity

In comparison, the cyclic voltammetry of precursor compound **1** revealed reversible first and second oxidations at $E^{o'} = +0.22$ and $+0.73$ V, respectively (Fig. 7). Additionally, the ΔE_p values of both redox processes are comparable to that of the Fc/Fc^+ couple, indicating a reversible one-electron transfer process. In summary, compounds **1**, **2** and **3** undergo porphyrin-centered first and second oxidations, and that these redox potentials are well within the $E_{1/2}(1) = \sim 0.81$ vs SCE obtained for the related (OEP)Ru(CO)(py)[41] and (TPP)Ru(CO)(py) [40] compounds. (Note: 0.81 V converts to ~ 0.35 V *vs* Fc/Fc^+ couple [42]). A second oxidation potential, $E_{1/2}(2)$ was recorded at 1.36 V *vs* SSCE (~ 0.90 V vs. Fc/Fc^+ couple) for (TPP)Ru(CO)(py) [40]. Similar redox behaviors were observed previously in some six-coordinate (por)Ru complexes [17, 18, 43].

Conclusion

We have prepared two ruthenium(II) octaethylporphyrin complexes of the form (OEP)Ru(CO)(Q), (Q = Qnl (**2**), and QN (**3**) from (OEP)Ru(CO) and characterized them by IR, MS, UV–vis and ^{1}H NMR spectroscopy. We have determined the X-ray crystal structure of **2** that shows CO coordination to Ru at the axial position. The sixth coordination site is occupied by quinoline through the Qnl-N. In the crystal packing of one batch of the single crystals of **2** (i.e. **2A**) the axially bound Qnl ligands of adjacent complexes are close to each other at a distance of 3.55 Å. In another batch of single crystal sample, the CO groups on adjacent complexes are on the same side. We also determined the X-ray crystal structure of the precursor complex (OEP)Ru(CO) (**1**) that

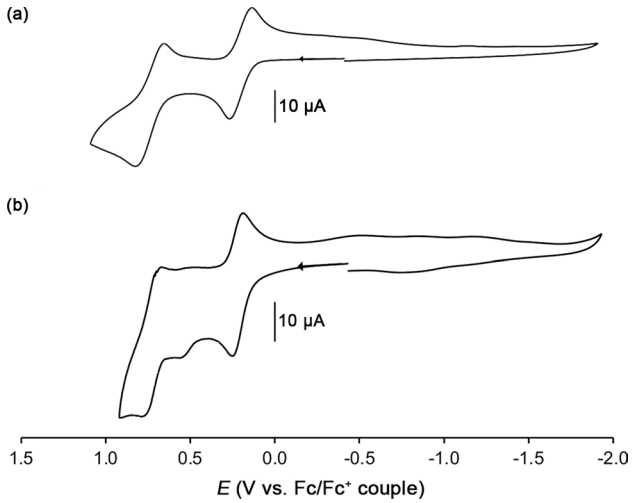

Fig. 6 Cyclic voltammogram of **2** (**a**) and **3** (**b**) showing the two oxidations. Conditions: 1 mM analyte, 200 mV/s scan rate, 0.1 M NBu_4PF_6 support electrolyte, room temperature

Table 4 Redox potentials of the compounds at a Pt working electrode.[a]

Compound	First oxidation	Second oxidation
1	+0.22	+0.73
2	+0.21	+0.74
3	+0.19	E_{pa} = +0.66 V; E_{pc} = +0.74 V

[a] Experiment conditions: 1 mM analyte, 0.1 M NBu_4PF_6, scan rate 0.2 V/s

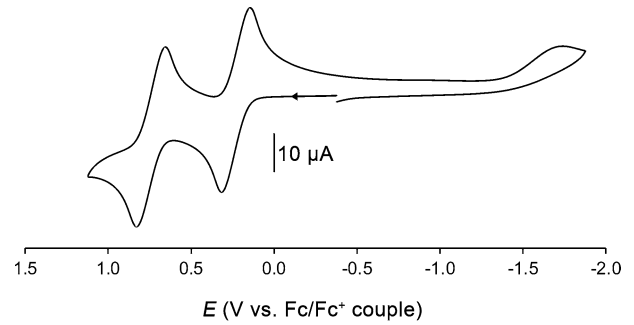

Fig. 7 Cyclic voltammogram of **1** showing the two oxidations. Conditions: 1 mM analyte, 200 mV/s scan rate, 0.1 M NBu_4PF_6 support electrolyte, room temperature

shows H_2O coordination at the axial position. The X-ray crystal structures of **1** and **2**, together with analysis of the spectroscopic data obtained suggest the site of binding of QN to Ru in the quinine complex **3** is likely through the quinoline N of QN. Electrochemical studies of the compounds via cyclic voltammograms revealed oxidations that are porphyrin-centered.

Supplementary Information The online version contains supplementary material available at https://doi.org/10.1007/s11243-023-00563-6.

Acknowledgements The authors thank the National Science Foundation (grant CHE-1726630) and the University of Oklahoma for funds to purchase the X-ray instrument and computers. The authors also thank the Fitchburg State University Special Projects Grant (grant T65-1230-T00-FCIN) and Fitchburg State University for funds for this project.

Author contributions D.A. performed experiments and wrote the main text of the manuscript.J.F.G. performed experiments and reviewed the manuscript.D.R.P. collected X-ray data, wrote the report and reviewed the manuscript.G.L. collected NMR data and reviewed the manuscript.

Declarations

Competing interests The authors declare no competing interests.

References

1. Afzal O, Kumar S, Haider MR, Ali MR, Kumar R, Jaggi M, Bawa S (2015) A review on anticancer potential of bioactive heterocycle quinoline. Eur J Med Chem 97:871–910. https://doi.org/10.1016/j.ejmech.2014.07.044
2. Mukherjee S, Pal M (2013) Medicinal chemistry of quinolines as emerging anti-inflammatory agents: an overview. Curr Med Chem 20(35):4386–4410. https://doi.org/10.2174/09298673113209990170
3. Matada BS, Pattanashettar R, Yernale NG (2021) A comprehensive review on the biological interest of quinoline and its derivatives. Bioorgan Med Chem 32:115973. https://doi.org/10.1016/j.bmc.2020.115973
4. Gorka AP, de Dios A, Roepe PD (2013) Quinoline drug-heme interactions and implications for antimalarial cytostatic versus cytocidal activities. J Med Chem 56(13):5231–5246. https://doi.org/10.1021/jm400282d
5. Weissbuch I, Leiserowitz L (2008) Interplay between malaria, crystalline Hemozoin formation, and antimalarial drug action and design. Chem Rev 108(11):4899–4914. https://doi.org/10.1021/cr078274t
6. Kapishnikov S, Hempelmann E, Elbaum M, Als-Nielsen J, Leiserowitz L (2021) Malaria pigment crystals: the Achilles′ Heel of the Malaria parasite. ChemMedChem 16(10):1515–1532. https://doi.org/10.1002/cmdc.202000895
7. de Villiers KA, Egan TJ (2021) Heme detoxification in the malaria parasite: a target for antimalarial drug development. Accounts Chem Res 54(11):2649–2659. https://doi.org/10.1021/acs.accounts.1c00154
8. de Dios AC, Tycko R, Ursos LMB, Roepe PD (2003) NMR studies of chloroquine−ferriprotoporphyrin IX complex. J Phys Chem A 107(30):5821–5825. https://doi.org/10.1021/jp0342982
9. Alumasa JN, Gorka AP, Casabianca LB, Comstock E, de Dios AC, Roepe PD (2011) The hydroxyl functionality and a rigid proximal N are required for forming a novel non-covalent quinine-heme complex. J Inorg Biochem 105(3):467–475. https://doi.org/10.1016/j.jinorgbio.2010.08.011
10. Constantinidis I, Satterlee JD (1988) UV-visible and carbon NMR studies of quinine binding to urohemin I chloride and uroporphyrin I in aqueous solution. J Am Chem Soc 110(3):927–932. https://doi.org/10.1021/ja00211a037
11. de Villiers KA, Gildenhuys J, le Roex T (2012) Iron(III) protoporphyrin IX complexes of the antimalarial cinchona alkaloids

quinine and quinidine. ACS Chem Biol 7(4):666–671. https://doi.org/10.1021/cb200528z
12. Gildenhuys J, Sammy CJ, Müller R, Streltsov VA, le Roex T, Kuter D, de Villiers KA (2015) Alkoxide coordination of iron(iii) protoporphyrin IX by antimalarial quinoline methanols: a key interaction observed in the solid-state and solution. Dalton Trans 44(38):16767–16777. https://doi.org/10.1039/C5DT02671G
13. Kuter D, Streltsov V, Davydova N, Venter GA, Naidoo KJ, Egan TJ (2016) Solution structures of chloroquine–ferriheme complexes modeled using MD simulation and investigated by EXAFS spectroscopy. J Inorg Biochem 154:114–125. https://doi.org/10.1016/j.jinorgbio.2015.06.010
14. Buller R, Peterson ML, Almarsson Ö, Leiserowitz L (2002) Quinoline binding site on malaria pigment crystal: a rational pathway for antimalaria drug design. Cryst Growth Des 2(6):553–562. https://doi.org/10.1021/cg025550i
15. Sanders JKM, Bampos N, Clyde-Watson Z, Darling SL, Hawley JC, Kim H-J, Mak CCM, Webb SJ (2000) In: Kadish K, Smith KM, Guillard, R (eds) The Porphyrin Handbook, Vol. 3 Academic Press, New York, p. 1–48. And references therein.
16. Buchler JW, Dreher C, Künzel FM (1995) Synthesis and coordination chemistry of noble metal porphyrins. Metal Complexes with Tetrapyrrole Ligands III. Berlin, Heidelberg: Springer Berlin Heidelberg, 1–69. And references therein.
17. Awasabisah D, Xu N, Sharmah Gautam KP, Powell DR, Shaw MJ, Richter-Addo GB (2013) Stable ruthenium nitrosyl porphyrins with axial O-bonded ligands; preparation and redox behavior. Dalton Trans 42(24):8537–8540. https://doi.org/10.1039/C3DT33109A
18. Awasabisah D, Xu N, Gautam KPS, Powell DR, Shaw MJ, Richter-Addo GB (2016) Preparation, characterization, electrochemistry, and infrared spectroelectrochemistry of ruthenium nitrosyl porphyrins containing η^1-o-bonded axial carboxylates. Eur J Inorg Chem 4:509–518. https://doi.org/10.1002/ejic.201501115
19. Cheng L, Richter-Addo GB (2000) Binding and activation of nitric oxide by metalloporphyrins and heme. In: Kadish KM, Smith KM, Guilard R (eds) The Porphyrin Handbook, vol 4. Academic Press, New York, pp 219–291 (**And references therein**)
20. Barley M, Dolphin D, James BR, Kirmaier C, Holten D (1984) Picosecond flash photolysis of carbonyl complexes of ruthenium(II) porphyrin pi cation radicals. J Am Chem Soc 106(14):3937–43
21. Bruker Nano, Inc. Data Collection: APEX3. Madison, Wisconsin: Bruker Nano Inc. 2018.
22. Bruker Nano, Inc. Data Reduction SAINT. Madison, Wisconsin: Bruker Nano Inc; 2016.
23. Rillema DP, Nagle JK, Barringer LF, Meyer TJ (1981) Redox properties of metalloporphyrin excited states, lifetimes, and related properties of a series of para-substituted tetraphenylporphine carbonyl complexes of ruthenium(II). J Am Chem Soc 103(1):56–62. https://doi.org/10.1021/ja00391a013
24. Krause L, Herbst-Irmer R, Sheldrick GM, Stalke D (2015) Comparison of silver and molybdenum microfocus X-ray sources for single-crystal structure determination. J Appl Crystallogr 48(1):3–10. https://doi.org/10.1107/S1600576714022985
25. Sheldrick GM (2015) *SHELXT*– Integrated space-group and crystal-structure determination. Acta Crystallogr A 71(1):3–8. https://doi.org/10.1107/S2053273314026370
26. Sheldrick GM (2015) Crystal structure refinement with *SHELXL*. Acta Crystallogr C 71(1):3–8. https://doi.org/10.1107/S2053229614024218
27. Macrae CF, Sovago I, Cottrell SJ, Galek PTA, McCabe P, Pidcock E, Platings M, Shields GP, Stevens JS, Towler M, Wood PA (2020) Mercury 4 0: from visualization to analysis, design and prediction. J Appl Crystallogr 53(1):226–35. https://doi.org/10.1107/S1600576719014092
28. Eaton GR, Eaton SS (1997) Reversible carbon monoxide binding by ruthenium carbonyl porphyrins. J Am Chem Soc 97(1):235–236. https://doi.org/10.1021/ja00834a066
29. Chow BC, Cohen IA (1971) Derivatives of tetraphenylporphineruthenium (II). Bioinorg Chem 1(1):57–63. https://doi.org/10.1016/S0006-3061(71)80001-7
30. Abraham RJ, Medforth CJ (1988) The NMR spectra of the porphyrins 36—Ring currents in octaethylporphyrin, meso-tetraphenylporphyrin and phthalocyanine complexes. Magn Reson Chem 26(9):803–12
31. Gouterman M (1978) Optical spectra and electronic structure of porphyrins and related rings. In: Dolphin D (ed) The porphyrins. Academic Press, pp 1–165
32. Sangster AW, Stuart KL (1965) Ultraviolet spectra of alkaloids. Chem Rev 65(1):69–130. https://doi.org/10.1021/cr60233a003
33. Antipas A, Buchler JW, Gouterman M, Smith PD (1978) Synthesis and optical and electronic properties of some ruthenium and osmium octaethylporphyrins. J Am Chem Soc 100(10):3015–3024. https://doi.org/10.1021/ja00478a013
34. Headen TF, Howard CA, Skipper NT, Wilkinson MA, Bowron DT, Soper AK (2010) Structure of π−π interactions in aromatic liquids. J Am Chem Soc 132(16):5735–5742. https://doi.org/10.1021/ja909084e
35. Salzmann R, McMahon MT, Godbout N, Sanders LK, Wojdelski M, Oldfield E (1999) Solid-State NMR, crystallographic and density functional theory investigation of Fe−CO and Fe−CO analogue metalloporphyrins and metalloproteins. J Am Chem Soc 121(16):3818–3828. https://doi.org/10.1021/ja9832818
36. Shirokova VV, Tyurin VS, Stanetskaya NM, Sokolova MN, Shkirdova AO, Zamilatskov IA (2019) The structure of complexes of carbonylruthenium(II) with octaethylporphyrin. Prot Met Phys Chem S 55(6):1104–1112. https://doi.org/10.1134/S2070205119060285
37. Hopf FR, O'Brien TP, Scheidt WR, Whitten DG (1975) Structure and reactivity of ruthenium(II) porphyrin complexes. Photochemical ligand ejection and formation of ruthenium porphyrin dimers. J Am Chem Soc 97(2):277–81
38. Rebouças JS, Cheu ELS, Ware CJ, James BR, Skov KA (2008) Synthetic and mechanistic aspects of a new method for ruthenium-metalation of porphyrins and schiff-bases. Inorg Chem 47(17):7894–7907. https://doi.org/10.1021/ic800616q
39. Collman JP, Barnes CE, Brothers PJ, Collins TJ, Ozawa T, Gallucci JC, Ibers JA (1984) Oxidation of ruthenium(II) and ruthenium(III) porphyrins Crystal structures of μ-oxo-bis[(p-methylphenoxo)(meso-tetraphenylporphyrinato)ruthenium(IV)] and ethoxo(meso-tetraphenylporphyrinato)(ethanol) ruthenium(III)-bisethanol. J Am Chem Soc 106(18):5151–63
40. Brown GM, Hopf FR, Ferguson JA, Meyer TJ, Whitten DG (1973) Metalloporphyrin redox chemistry. Effect of extraplanar ligands on the site of oxidation in ruthenium porphyrins. J Am Chem Soc 95(18):5939–42
41. Barley M, Becker JY, Domazetis G, Dolphin D, James BR (1981) Redox chemistry of ruthenium porphyrins: evidence for internal electron transfer and the characterization of [Ru(OEP+˙)] species. J Chem Soc Chem Comm 19:982–983. https://doi.org/10.1039/C39810000982
42. Connelly NG, Geiger WE (1996) Chemical redox agents for organometallic chemistry. Chem Rev 96(2):877–910. https://doi.org/10.1021/cr940053x
43. El-Attar MA, Xu N, Awasabisah D, Powell DR, Richter-Addo GB (2012) Cyclic voltammetric and fiber-optic infrared spectroelectrochemical studies of six-coordinate (por)Ru(NO)Cl compounds (por = porphyrinato dianion). Polyhedron 40(1):105–109. https://doi.org/10.1016/j.poly.2012.03.034